Nautical Disaster: An Autonomous Surface Vessel

Sabrina Button, William Palacek, Aedan Loughran, Angus Dickson, Jai Moraes, Logan Calder, Spencer Osborn, Julian Tiqui

***Abstract*—aQuatonomous presents *Nautical Disaster*, an Autonomous Surface Vessel (ASV) designed for the 2025 RoboBoat competition. The structural design features a foam-plywood layered hull and plywood bridge, with an azimuth-controllable propulsion system. The ASV uses an M10 GPS, 6-Axis IMU, Unitree 4D LiDAR, and two fisheye lens cameras (bow and starboard). Autonomous decision-making is powered by an NVIDIA Jetson Nano running ROS2, with actuator control managed by a Pixhawk 4 autopilot through MAVROS, which connects ROS2 to the MAVLink system. Vision-based motion control identifies buoys based on camera segments, while the LiDAR, segmented into three z-levels, aids in course localization. Communication is managed via a redundant telemetry system with ground station access over radios or WiFi, and manual control via RC. The system includes remote and physical E-stop capabilities. The perception and autonomy systems have been tested in Python and Gazebo simulations, with buoyancy and actuation tested in Lake Ontario.**

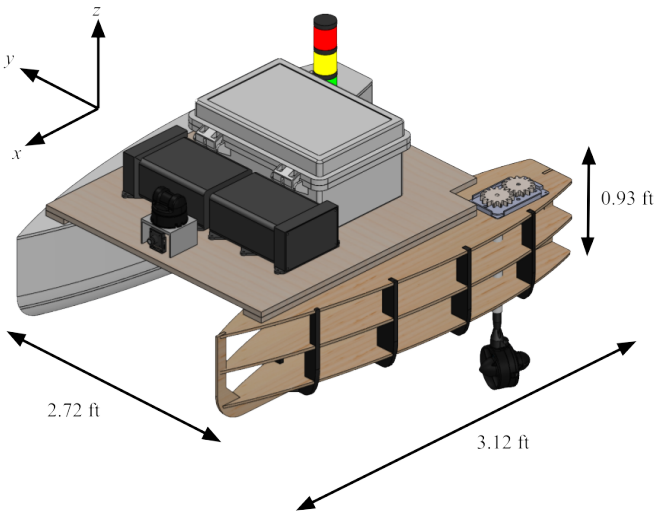

Fig. 1. A complete CAD rendering of the Nautical Disaster ASV, featuring one pontoon in a deconstructed view to reveal its internal structural framework.

I. Competition Strategy

A. Adherence to Mechanical Constraints

The vessel, pictured in Fig. 1, is designed to comply with competition constraints while maximizing bridge space and load capacity to accommodate electrical components. The main structure of the vessel measures 3.12 ft long, 2.72 ft wide and 0.93 ft tall. A closed-cell foam core hull wrapped with fiberglass is used to minimize weight while retaining shape and durability [1], [2]. The vessel has a mass of 40 lbs. The maximum load capacity is 140 lbs and the optimal load is 55–70 lbs. To facilitate transportation to the competition, the bridge, electrical system, and hulls are designed to be modular and detachable from one another.

B. Sensor Selection

The ASV's sensing system is designed to perform autonomy tasks using a minimal number of strategically placed sensors, prioritizing simplicity. An M10 GPS and 6-Axis ICM-20689 IMU onboard a Pixhawk 4 Autopilot are used to localize the ASV in the global environment using an extended Kalman filter [3]. A secondary 9-Axis IMU is wired to a Jetson Nano microcontroller for measurement redundancy given the sensor noise present in the Pixhawk's onboard IMU.

A Unitree 4D LiDAR L1 is mounted on the bow of the ASV for obstacle detection and assistance with various tasks. The 3D LiDAR allows for objects to be identified based on their height, negating the need for sensor fusion in environmental identification tasks, which is an advantage over a 2D LiDAR.

A 180-degree fish-eye lens camera is mounted on the bow of the ASV for detecting buoys in front of the ASV and steering based on their position. Using a wide-angle lens maximizes the field of view at the cost of some distortion. However, it eliminates the need for multiple cameras on the bow, reducing power consumption and simplifying integration. A second 180-degree fish-eye lens camera is mounted on the starboard of the ASV for viewing signals and signage without having to maneuver the ASV, which is relevant to Task 3 and Task 4.

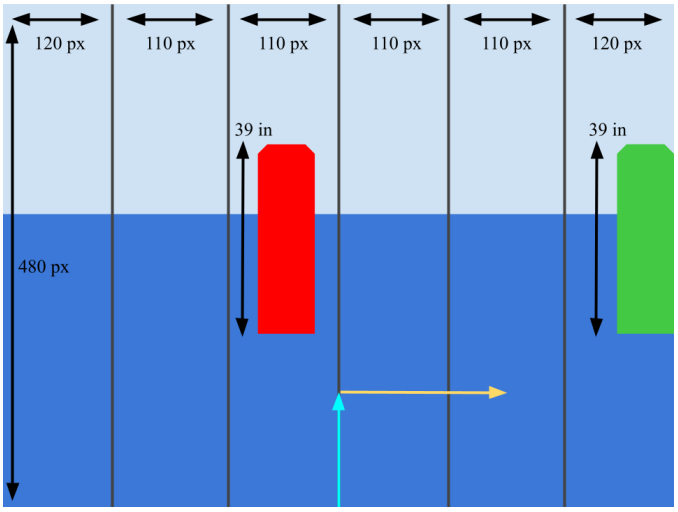

Fig. 2. A camera 6-window segment example for a situation in which the ASV must navigate between a red buoy (right) and a green buoy (left). The cyan arrow indicates the heading of the ASV. The yellow arrow indicates the turning vector of the ASV required to get on the desired course, given the window segments that each buoy currently occupies.

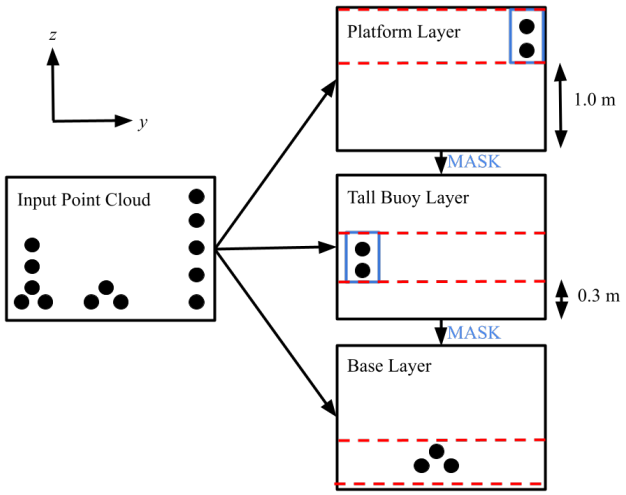

Fig. 3. A Y-Z plane cross-section of the LiDAR segmentation approach in which an input point cloud is split into three layers based on point heights. Upper layers create bounding boxes (blue) around their points, which mask out points on lower layers that are aligned on the X-Y plane. Each point cloud layer is flattened after the segmentation is complete.

C. Simple Perception-Based Approach to Decision-Making

1) Camera Windowed Segmentation: Individual frames from the bow camera are divided into six near-equal vertical segments. Buoys in the camera frame are mapped to a segment corresponding to their location within the image. The color and size of a buoy and its segment index within the frame indicate the ASVs next desired movement. For example, if the ASV is attempting to navigate between two buoys and observes that the leftmost buoy is in the segment nearest to the middle left of the frame, while the right buoy is on the farthest right segment, the ASV must steer right. The goal is to steer the ASV to maintain the buoys at equal positions on opposite sides of the camera frame. This example is presented in Fig. 2. This simple algorithm is robust and imposes a lower computational burden compared to an ML/AI system.

2) Three level LiDAR segmentation: The 3D LiDAR system is divided into three height-based sections, which are then flattened to simplify the algorithmic processing of the LiDAR data. The first section captures objects up to 0.3 m above the waterline, primarily small buoys; the second captures objects between 0.3 m and 1.0 m, such as tall buoys; and the third captures objects above 1 m, including platforms. Higher layers use bounding boxes to mask out points from lower layers, ensuring that each object appears only on its corresponding height layer, as shown in Fig. 3. This approach allows objects to be uniquely identified based on their respective layers. This system supplements camera-based detection, serving as a secondary environmental sensing method. Obstacle detection utilizes a combined point cloud of all three layers, ensuring all objects are identified and avoided. The classification of buoys by height and the identification of platforms is particularly applicable to Task 1 and Task 3.

D. Approach to Tasks

The ASV employs a potential field algorithm for obstacle avoidance by assigning positive charges to the vessel and obstacles, proportional to their pixel size in the camera view, and a negative charge to the goal [4]. This is used to avoid yellow buoys (Task 2), black buoys (Task 4), and in return home (Task 6). Left-right buoy navigation utilizes the vertically segmented 180 degree camera on the bow with color detection to classify and align red buoys left and green buoys right, ensuring forward progress; applied in Tasks 1 and 2. The speed challenge employs camera-based detection of the start signal via the starboard camera, initiating movement upon signal activation. Apex turning is executed around the blue buoy once its size and segment position

Fig. 4. The two twin pontoons after the skeleton is layered with XPS foam, before fiberglassing. Spray foam is used to seal any gaps.

in the bow camera align with predefined parameters (Task 4). Oil spill tracking utilizes height-segmented LiDAR data, clustering first-layer buoy points to count the number of clusters. The count is adjusted by subtracting one to exclude the blue buoy used for apex turning (Task 4). The count maybe observed in a graphical interface hosted by the speed challenge node. Docking leverages a frontal camera for navigation, the starboard camera for symbol recognition, and LiDAR for precise edge detection, enabling symbol-based docking alignment (Task 3). Task 5 is not attempted. For returning home, a camera-driven potential fields method integrates GPS-based path planning for dynamic obstacle avoidance and waypoint optimization (Task 6).

II. Design Strategy

A. Hull Design and Construction

To maximize surface area and stability, a twin hull-design is used [5], [6]. Both hulls measure 3.1 ft long, consisting of five layers of XPS foam board layered between ¼ in plywood sheet laser cut for precision. The foamed hulls before sealing are presented in Fig. 4. To increase the structural strength, the hulls are supported by a plywood keel and 3D printed frames as presented in Fig. 1. The hulls are sanded and wrapped in fiberglass and epoxy resin to ensure rigidity and waterproofing.

B. Bridge Layout and Design

The 27 in $\times$ 24 in bridge is built from ½ in marine plywood for its resistance to water permeability and its high strength properties [7]. The pontoon hulls are attached using six threaded inserts and bolts for a strong connection and easy detachment for transportation. The bridge layout, seen in Fig. 1, is optimized for shorter cable lengths and unrestricted access to all components. The large bridge enables reusability in future years by accommodating additional equipment and can support 140 lbs, per density-buoyancy calculations.

C. Waterproofing and Degradation Prevention

The use of marine grade plywood and polyurethane paint increases the longevity of the vessel [7], [8]. The solid hull structure is designed to provide an additional layer of redundancy preventing the vessel from taking on water if it is pierced. Electrical components are safely stored in the electrical box and battery box which use O-rings and cord grips to prevent water ingress [9]. Each box has an elevated base to further reduce potential water damage. The electrical box also includes a removable second floor made from clear plexiglass, which allows a more accessible and organized interior.

D. Propulsion System

The propulsion system presented in Fig. 5 is designed with a focus on maneuverability, ease of maintenance, and safety, following typical marine practices [10]. On each pontoon, a steering shaft capable of 180 degrees of rotation is controlled by two STP-MTR-23055 SureStep stepper motor placed within the pontoon. Stepper motors are selected for their precise position control. Each shaft is surrounded by a ¾ in PVC tube and attached to a T200 Blue Robotics Thruster. Two gears with a ratio of 1:1 join the steppers to the steering shaft and are covered with a transparent case anytime the vessel is in use.

E. Autonomy and Control System

The autonomy and control system uses a Jetson Nano running ROS2 Foxy to handle decision-making algorithms and perception tasks, with LiDAR and cameras directly connected to the computer. Navigation and control commands, such as desired positions and velocity vectors, are transmitted to a Pixhawk 4 autopilot via MAVROS over

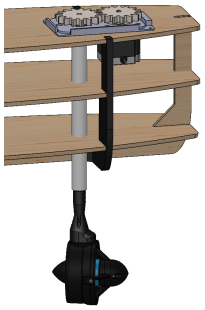

Fig. 5. The propulsion system of the ASV, where a stepper motor controls the direction of a T200 thruster at the end of a PVC pipe through the pontoon with a 1:1 gear ratio.

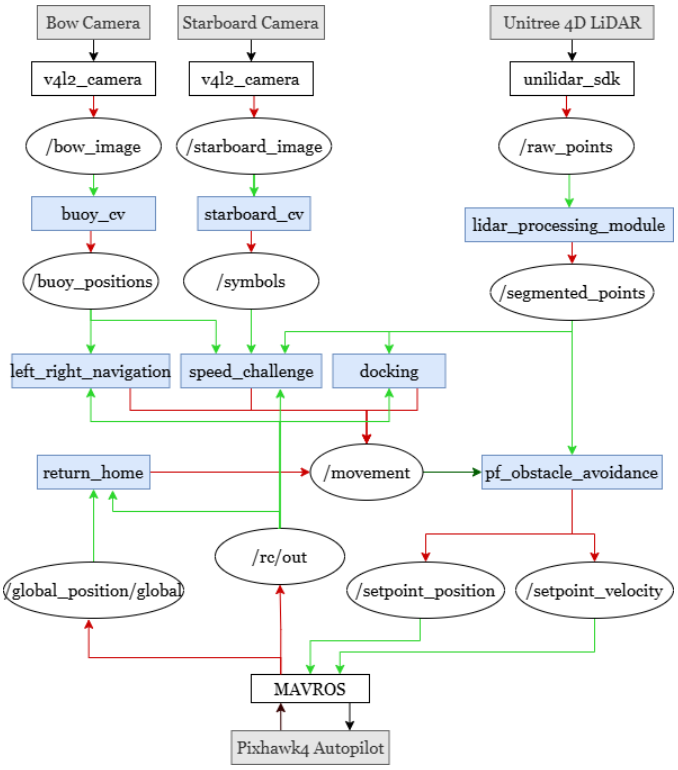

Fig. 6. The ROS architecture of the ASV, where ovals represent ROS topics. White rectangles represent driver ROS nodes, blue rectangles represent nodes developed by the team and discussed in this paper, and gray rectangles represent physical hardware. Subscriptions are shown as green arrows, and publishing is represented by red arrows.

UART. MAVROS facilitates communication with the MAVLink-based autopilot, streamlining navigation, telemetry, and mission execution. The Pixhawk, selected for its integrated control capabilities, simplifies the overall system, allowing more emphasis on developing high-level algorithms rather than managing low-level controls.The integrated system architecture is illustrated in Fig. 6.

The Pixhawk 4 interfaces with the propulsion system, using pulse width modulation (PWM) signals to control stepper drivers and thruster ESCs. It provides localization data to the Jetson Nano and employs a proportional-integral-derivative (PID) controller to compute actuator commands for achieving target positions. The Pixhawk is loaded with a rover-style frame as a model of the vehicle; One output channel is mapped to steering, and a second is mapped to thrust. Both thrusters and both stepper motors receive duplicate inputs from the Pixhawk controller to simplify maneuvers, as presented in Fig. 7.

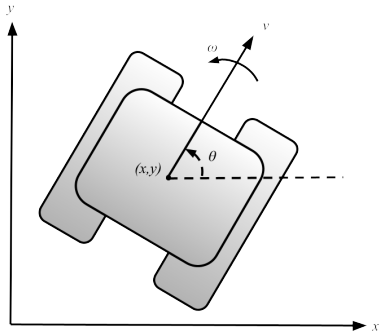

Fig. 7. The control model of the ASV, where v represents thrust and ω represents steering (angular velocity). The vehicle state is represented by $[x, y, \theta]$.

F. Computer Vision

1) Buoy Detection: Buoy detection and range estimation utilize HSV color segmentation to identify target colors (red, yellow, green) and bounding box analysis for localization. Using the known buoy dimensions, a calibrated pixel-to-distance ratio determines the distance based on bounding box size, leveraging perspective projection principles [11]. This approach enables approximately 0.2 m accuracy in obstacle localization.

2) Symbol Identification: In the speed challenge, the starboard camera navigates the ASV to the correct starting position by detecting a high number of red pixels, initiating motion when the number of green pixels matches the initial number of red pixels. The course is managed using segmented frames from the bow camera. For the docking challenge, shape recognition of circles, squares, triangles, and plus signs is achieved using OpenCV: Circle detection utilizes the Hough Circle Transform, squares and rectangles are identified via contour approximation and aspect ratio, triangles by contour fitting

with three vertices, and plus signs by detecting intersecting rectangles or lines; Color detection is performed through RGB thresholding.

G. Telemetry System

Ground station communication with the ASV is supported by four redundant methods to ensure reliable connectivity. The Jetson Nano, connected to the Pixhawk 4 via UART, can be accessed over Wi-Fi using Ubiquiti Wi-Fi bullets, allowing the user to control the Pixhawk through ground control software on the Jetson. Alternatively, the user can run ground control software on a laptop and connect to the Pixhawk via a Sik telemetry radio link. Manual control is available through an RC controller with preset mappings. Additionally, a remote E-stop system enables actuator shutdown via signals sent between ground and onboard Elgoo HC-12 transceivers.

Both ground station and onboard setups for all four described redundant systems use LoRaWAN antennas, enabling remote operation up to 3 km away.

H. Power and Safety System

The power system prioritizes reliability. Components and wiring are protected against overcurrent and overvoltage through blade fuses and voltage regulators. Preliminary calculations, including thruster tests, indicate a current draw of 10—15 A at full throttle. The estimated battery life is 27.2 minutes under typical operating conditions, as concluded by the power consumption analysis in Table I.

TABLE I
POWER CONSUMPTION AND BATTERY LIFE ANALYSIS

Component	# of Components	Current Draw (A)	Voltage (V)	Power (W)
Telem: Pixhawk + Jetson	1	7.00	5	36.76
WiFi Bullet	1	0.29	24	8.75
LiDAR	1	0.50	12	7.05
Signal Tower	1	0.167	12	2.35
HC-12 Nano E-stop	1	0.33	9	3.00
T200 Thruster (Theoretical)	2	22.00	15.26	671.44
STP-MTR-23055 Stepping Motor	2	2.80	15.26	85.46
Totals	-	57.89	-	814.81
Battery Life (hrs) @ Full Power		0.36 (21.8 Minutes)		
Battery Life (hrs) @ 80% Power Output		0.45 (27.2 Minutes)		

Two 14.8 V 10 Ah batteries are connected in parallel to form the main power line, which passes through a 100 A-rated Solid State Relay (SSR) and the fuse block Power Distribution Module (PDM). The positive line connects through the main line SSR into PDM as shown in the relay-actuator system. The negative bus line of the fuse block connects to the negative terminal block allowing a complete circuit back to the batteries. The PDM is rated for up to 125 A and 32 V DC and will be running the nine individual sub-circuits in the ASV of its available 12 circuits. SSRs use semiconductor materials to control power output via photonic activation when a control voltage of 3–32 V is applied across their terminals. The E-stop button controls an internal switch rated for 10A, regulating the 9V Alkaline battery control voltage across the relay. Of the nine circuits, those not requiring battery voltage are regulated to their appropriate levels, trading off power efficiency for component longevity.

Relays enable instant power cutoff to the stepper motors and thrusters, ensuring safety. SSRs control the thrusters, while an electro-photonic relay manages SSRs and stepper driver power, as it cannot handle the thruster current. The Jetson Nano controls the relay system via designated pins, enabling actuator power shutdown remotely through the mentioned redundant communication options. The remotely controlled E-stop system utilizes Elgoo HC-12 transceivers to send stop signals to the actuators. This system halts actuator operation without cutting power to the entire system, ensuring other subsystems remain operational.

The system's actuators may also be stopped using a soft E-stop using the ground station software connected to the Pixhawk 4, or using the designated stop button on the RC controller. This E-stop is considered separate from the physical actuator E-stop enabled by the Jetson relay connection. A schematic of the complete power system is provided in Appendix A.

III. TESTING STRATEGY

A. Software Simulation

1) Algorithmic Simulations in Python: The team developed a modular Python-based algorithm visualizer using Pygame to test and refine custom path planning algorithms. Fig. 8 shows the tool using the A* algorithm. Multiple algorithms can be tested and switched via a built-in launcher, with plans to iterate on the potential field algorithm for future designs.

2) Perception Simulations in Gazebo: A virtual competition space was created using Gazebo to test buoy identification within camera segments, and

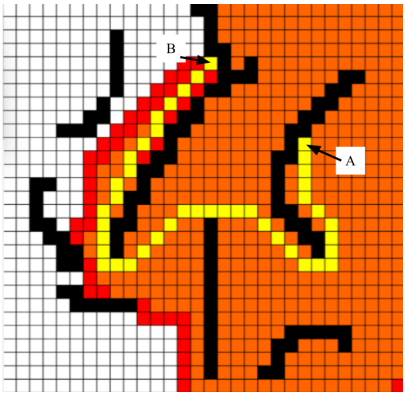

Fig. 8. A screen capture of the cell-based Python simulation for path finding algorithms, with an A* planner active. Black cells represent obstacles, orange and red cells represent the open and closed lists of cells, and yellow cells represent the optimal path from point A to point B.

the segmentation of LiDAR point clouds based on height. This enables evaluation of the perception system without the system being prepared for outdoor testing.

B. Structural Testing

Initially, SolidWorks flow simulations and FEA analyses were performed on the vessel's CAD model to ensure hydrodynamic structure, buoyancy, and strength. A 1:3 scale model of the bridge and pontoons was constructed to test buoyancy and fiberglass layup techniques. This involved materials testing on adhesives, foam, and plywood to determine the optimal surface roughness of the foam for bonding to the pontoon skeleton. An 8x2 in foam sample submerged for a week showed no weight change, confirming non-absorbent properties. GPS accuracy was verified within the electrical box to ensure unobstructed performance [12]. Propulsion testing will be conducted in a wave basin before competition to compare measured thrust against theoretical thrust (11.6 lb/ft) under varying water roughness conditions.

C. Electrical Bench Tests

Testing is compartmentalized to assess component performance before validating full subsystem functionality. Propulsion tests evaluate steppers and thrusters individually, measuring current draw and torque to optimize power consumption and battery health. Thrusters are tested at 14.8 V with varying torque and speed, analyzing the torque-speed curve. Telemetry testing evaluates Pixhawk directional and speed responses via direct serial and radio telemetry connections, with communication tested across a 1–500 m range. All three active radio-antenna systems are tested simultaneously to ensure no interference. The mainline E-stop is tested for proper circuit interruption, while the relay system is validated by disabling power and PWM signals to individual and all actuators to check isolation. The Elgoo HC-12 remote E-stop is tested at expected and maximum operational ranges (1–1000 m) for functionality.

D. Autonomous Experimentation in a Wave Basin

The team has access to a laboratory with a wave-controllable basin for testing. Subsystem testing will begin with manual operation via RC controller to verify thruster and azimuth stepper functionality. Next, waypoints will be sent from ground control software using SiK telemetry radios and SSH into the Jetson Nano to validate the PID control system and the Pixhawk's ASV model. Before autonomous testing, the perception system will be verified by SSHing into the Jetson Nano to confirm accurate segmentation from the bow camera and LiDAR. Autonomous navigation will be tested by monitoring buoy navigation nodes as the ASV navigates between buoys under varied starting positions, angles, and wave conditions.

At each stage—manual, waypoint, and autonomous mode—all E-stop systems (remote actuator, Jetson-controlled, soft, and physical) will be triggered to confirm proper operation.

ACKNOWLEDGMENTS

Acknowledgment is given to the Stephen J.R. Smith Faculty of Engineering, Seaspan ULC, Honeywell, Adaptive Marine Solutions Ltd., Claigan Environmental, Sensor Technology Ltd., and the Alma Matter Society of Queen's University's Sustainability Commission for their generous financial contributions. The Engineering Society of Queen's University is recognized for providing design bay space and operational support. Gratitude is extended to Dr. Joshua Marshall and Ph.D. Candidate Thomas Sears from Ingenuity Labs for technical advice and paper review, as well as to Dr. Ryan Mulligan and Ph.D. Candidate Thomas Penderghast from the Beaty Water Research Center for access to the wave basin and water research guidance.

REFERENCES

[1] F. T. Wallenberger and P. A. Bingham, *Fiberglass and Glass Technology*. Springer, 2010.

[2] J. Xiong, Y. Du, D. Mousanezhad, M. E. Asl, J. Norato, and A. Vaziri, "Sandwich structures with prismatic and foam cores: A review," *Advanced Engineering Materials*, vol. 21, no. 1, p. 1800036, 2019.

[3] Pixhawk, "Pixhawk 4 flight controller," https://docs.px4.io/main/en/flight_controller/pixhawk4.html, 2021, accessed: 2025-01-22.

[4] P. Allen, "Potential field navigation," https://www.cs.columbia.edu/ allen/F17/NOTES/potentialfield.pdf, 2017, accessed: 2025-01-22.

[5] H. S. Chan, "Prediction of motion and wave loads of twin-hull ships," *Marine Structures*, vol. 6, no. 1, pp. 75–102, 1993.

[6] R. I. Julianto, T. Muttaqie, R. Adiputra, S. Hadi, R. L. L. G. Hidajat, and A. R. Prabowo, "Hydrodynamic and structural investigations of catamaran design," *Procedia Structural Integrity*, vol. 27, pp. 93–100, 2020.

[7] W. Tucker, *Nonmetallic Materials in Marine Service*. John Wiley & Sons, Ltd, 2022, ch. 16, pp. 421–439.

[8] A. Das and P. Mahanwar, "A brief discussion on advances in polyurethane applications," *Advanced Industrial and Engineering Polymer Research*, vol. 3, no. 3, pp. 93–101, 2020.

[9] P. H. Corporation, *Parker O-Ring Handbook*, 2007.

[10] J. W. Group, *Marine Propulsion Guide*, 2010.

[11] R. Hartley and A. Zisserman, *Multiple View Geometry in Computer Vision*. Cambridge, UK: Cambridge University Press, 2004.

[12] S. J. Lee and T. H. Kim, "Study on the effectiveness of gps signal quality for autonomous marine navigation," *Ocean Engineering*, vol. 45, pp. 24–35, 2012.

APPENDIX A
ELECTRICAL SYSTEM SCHEMATIC

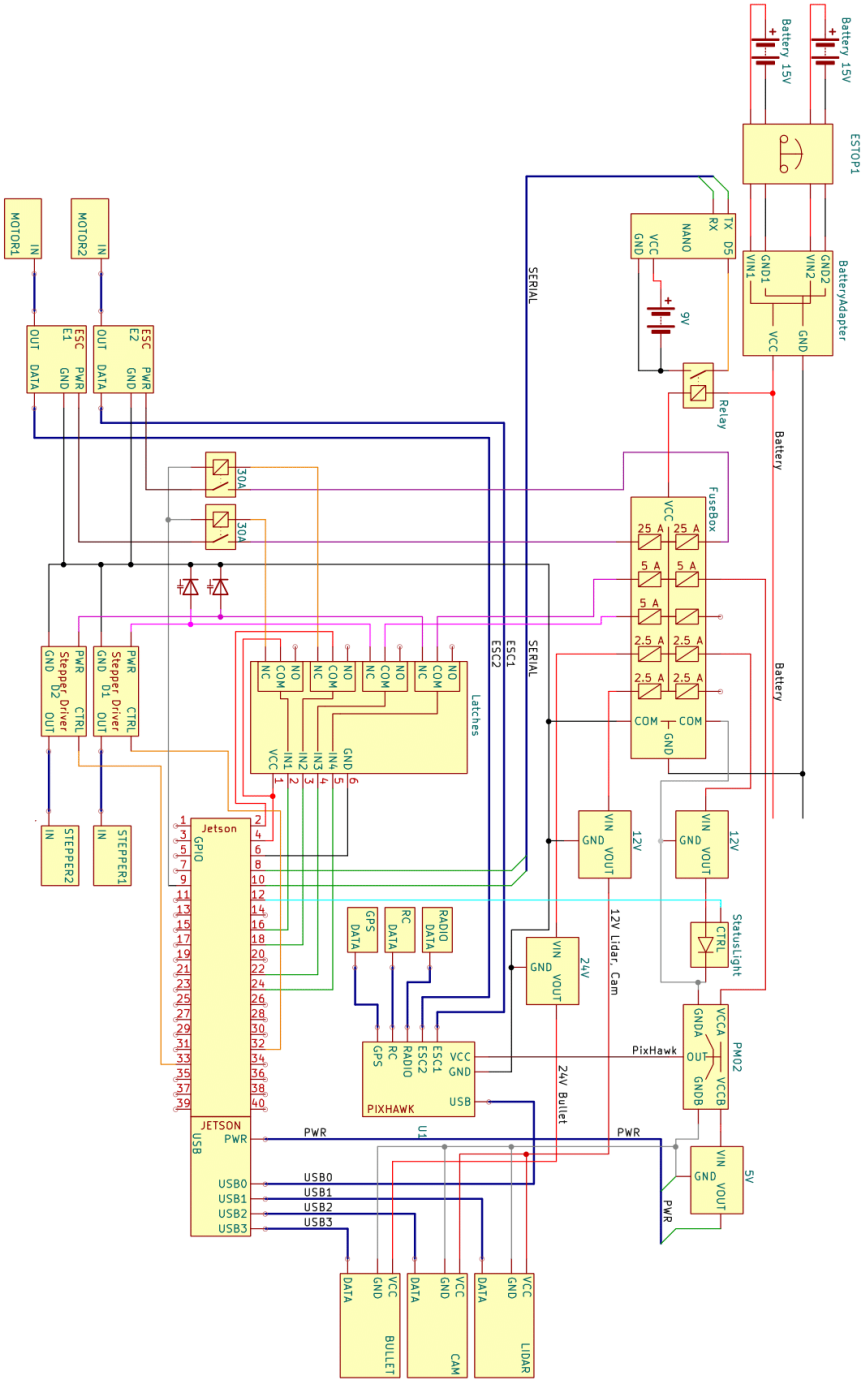

Fig. 9. A complete schematic of the Nautical Disaster electrical system.